Will the 1-bit GNSS receiver prevail?

Manuel Stein and Josef A. Nossek

Institute for Circuit Theory and Signal Processing
Technische Universität München, Germany
Email: {manuel.stein, josef.a.nossek}@tum.de

***Abstract*—In the context of satellite-based positioning, the problem of range-estimation with low resolution analog-to-digital conversion (ADC) is considered. While ADC with coarse output resolution degrades the positioning performance of Global Navigation Satellite System (GNSS) receivers, it's simplicity allows to realize sampling at high spatial and temporal rates in an energy and hardware efficient way. Therefore, here the achievable range-estimation accuracy of GNSS receive systems with 1-bit ADC resolution, multiple antennas and high receive bandwidths is analyzed. For different scenarios, including multi-path propagation and the presence of broadband interference, we investigate the scaling behavior of the estimation performance when increasing the number of receive antennas or the sampling rate. Results for all considered scenarios show that if a moderately higher number of antennas or a moderately faster temporal rate is used, 1-bit GNSS receive systems have the potential to outperform ideal receivers with infinite ADC resolution. This insight emphasizes that a receiver architecture with 1-bit ADC has the potential to play an important role for future low-cost receivers as well as for sophisticated energy efficient high-performance GNSS systems.**

***Index Terms*—1-bit ADC, signal parameter estimation, satellite-based positioning**

I. Introduction

The development of high-performance GNSS receive systems becomes challenging if one imposes strict constraints on the available power, chip-size or money budget. As the operation of critical infrastructure like mobile communication systems, electric distribution networks or financial trading systems can depend on correct time synchronization attained through a GNSS receive system, robustness against interference and multi-path propagation is another important requirement that should be met by the receiver design without violating the limitations defined by the available hardware. Under the assumption, that the receive system operates on the basis on an efficient estimation algorithm, two fundamental design options exist in order to attain higher positioning accuracy and robustness against channel imperfections like multi-path propagation or interference. One is to extend the amount of receive antennas, the other is to implement a higher receive bandwidth through a faster temporal sampling rate. However, these alternatives both increase the complexity of the receiver, especially as the ADC forms a bottleneck when heading at a low-complexity design [1]. With multiple receive sensors each antenna requires it's own radio front-end and therefore an individual ADC. High temporal sampling rates become inefficient at high amplitude resolution with b output bits as the power dissipation of the ADC increases exponentially $\mathcal{O}(2^b)$. An interesting approach which allows to simplify the design of the GNSS receive front-end in a radical way is to use ADC with 1-bit output resolution. If a symmetric hard-limiter is used to map the analog continuous-time signal to a digital discrete-time representation, the ADC device can be realized by a single comparator and does not require an automatic gain control (AGC) which adjusts the signal level at it's input. This reduces the complexity of the analog radio front-end associated with each receive sensor significantly. Further, basic digital signal processing operations involving the receive signal can be performed in an efficient way. For example, correlation of the receive signal with a local signal replica can be calculated without using multiplications. However, 1-bit ADC is a highly non-linear and non-bijective operation which inherently comes with a performance-loss. Fortunately, it turns out that for scenarios with low signal-to-noise ratios (SNR) like encountered in GNSS applications, the information-loss is tolerable with -1.96 dB. Therefore, on the one hand 1-bit ADC is an attractive option if one is interested in reducing the energy consumption and complexity of a mobile GNSS receive system. On the other, the simplicity of the front-end with 1-bit ADC can be used to realize receivers with multiple antennas and high sampling rates. As the amount of antennas and the receive bandwidth strongly determine the achievable positioning accuracy and the robustness against multi-path propagation and interference, a receiver architecture with 1-bit ADC also bears the potential to enable the development of robust high-performance receive systems with moderate energy and hardware requirements.

A. Contribution

In the light of the benefits which are provided by 1-bit ADC in the context of GNSS and the small associated performance-loss, the question arises if such a front-end architecture has the capability to dominate future GNSS receiver markets. Here we approach this aspect by investigating the performance of 1-bit GNSS systems when the number of antennas or the temporal sampling rate is increased. In particular we demonstrate the performance gains that can be achieved in critical scenarios with multi-path propagation and broadband interference. Results show that besides multiple antennas, the receive bandwidth is a crucial design criterion for robust high-performance GNSS receive systems. The possible performance gain clearly outweighs the loss introduced by coarse signal amplitude resolution. The envisioned 1-bit ADC front-

978-1-4799-3320-4/14/$31.00 © 2014 IEEE

end technology allows to exploit this conceptual degree-of-freedom for the receive system design in a highly efficient way.

B. Related Works

In [2] and [3] early discussions on signal quantization and estimation of signal parameters from quantized observations are found. In [4] [5] [6] the authors study channel parameter estimation based on a 1-bit quantizer. Quantization has also been discussed extensively in the area of communications and information theory. The authors in [7] showed, that the channel capacity of a quantized AWGN channel can be increased if the sampling rate is increased while in [8] the benefits of an adjusted quantization threshold is discussed. Recently, [9] derived a lower bound on the capacity of quantized MIMO channels with noise correlations. In the context of GNSS, [10] discusses quantization-losses and [11] considers the possibility to improve the SNR of the correlator output with a quantized receive signal by using high sampling rates and reducing the receive bandwidth. In [12] [13] it was shown that adjusting the analog pre-filter prior to the ADC allows to partially compensate the quantization-loss without increasing the digital complexity of the GNSS receive system.

II. System Model

On the following pages, we assume a GNSS receiver with an uniform linear array (ULA) which consists of M antennas. The antennas are placed with a spacing corresponding to half the carrier wavelength. Each antenna has an analog in-phase output $y_{I,m}(t) \in \mathbb{R}$ and an analog quadrature output $y_{Q,m}(t) \in \mathbb{R}$. The overall analog GNSS receive signal from all sensors can be written in vector notation by

$$\boldsymbol{y}(t) = \begin{bmatrix} \boldsymbol{y}_I^T(t) & \boldsymbol{y}_Q^T(t) \end{bmatrix}^T \in \mathbb{R}^{2M}, \tag{1}$$

with $\boldsymbol{y}_I(t) \in \mathbb{R}^M$, $\boldsymbol{y}_Q(t) \in \mathbb{R}^M$ and

$$\boldsymbol{y}_{I/Q}(t) = \begin{bmatrix} y_{I/Q,1}(t) & y_{I/Q,2}(t) & \dots & y_{I/Q,M}(t) \end{bmatrix}^T. \tag{2}$$

A. Receive Signal Model

The coherent and doppler-compensated receive model

$$\begin{aligned} \boldsymbol{y}(t) = &\boldsymbol{A}(\zeta_S)\boldsymbol{x}(t-\tau_S) + \gamma_P \boldsymbol{A}(\zeta_P)\boldsymbol{\Phi}(\phi_P)\boldsymbol{x}(t-\tau_P) + \\ &+ \boldsymbol{A}(\zeta_J)\boldsymbol{z}(t) + \boldsymbol{\eta}(t) \end{aligned} \tag{3}$$

is assumed to be comprised by a line-of-sight satellite signal $\boldsymbol{x}(t-\tau_S) \in \mathbb{R}^2$, a multi-path component $\boldsymbol{x}(t-\tau_P) \in \mathbb{R}^2$, broadband interference $\boldsymbol{z}(t) \in \mathbb{R}^2$ and sensor noise $\boldsymbol{\eta}(t) \in \mathbb{R}^{2M}$. The line-of-sight satellite signal $\boldsymbol{x}(t-\tau_S)$ impinges on the array under the angle $\zeta_S \in \mathbb{R}$ with time-delay $\tau_S \in \mathbb{R}$, while the multi-path component $\boldsymbol{x}(t-\tau_P)$ arrives attenuated by $\gamma_P \in \mathbb{R}$ with a time-delay $\tau_P \in \mathbb{R}$, angle $\zeta_P \in \mathbb{R}$ and phase-offset $\phi_P \in \mathbb{R}$. The interference $\boldsymbol{z}(t)$ results from a single broadband signal source which is located such that the signal arrives at the array with an angle of ζ_J. The described receive setup is depicted in Fig. 1. The steering matrix as a

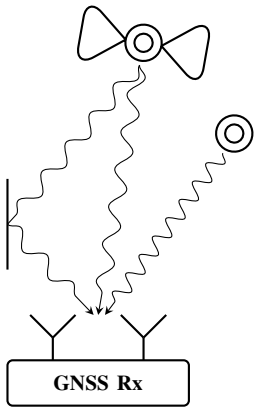

Fig. 1. GNSS receive setup with multi-path and interference

function of the angle-of-arrival ζ

$$\boldsymbol{A}(\zeta) = \begin{bmatrix} \boldsymbol{A}_I^T(\zeta) & \boldsymbol{A}_Q^T(\zeta) \end{bmatrix}^T \in \mathbb{R}^{2M \times 2}, \tag{4}$$

is determined by the steering matrix corresponding to the in-phase sensor outputs

$$\boldsymbol{A}_I(\zeta) = \begin{bmatrix} \alpha_1(\zeta) & \beta_1(\zeta) \\ \alpha_2(\zeta) & \beta_2(\zeta) \\ \vdots & \vdots \\ \alpha_M(\zeta) & \beta_M(\zeta) \end{bmatrix} \in \mathbb{R}^{M \times 2} \tag{5}$$

and the steering matrix associated with the quadrature outputs

$$\boldsymbol{A}_Q(\zeta) = \begin{bmatrix} -\beta_1(\zeta) & \alpha_1(\zeta) \\ -\beta_2(\zeta) & \alpha_2(\zeta) \\ \vdots & \vdots \\ -\beta_M(\zeta) & \alpha_M(\zeta) \end{bmatrix} \in \mathbb{R}^{M \times 2}, \tag{6}$$

where for both matrices the single entries are given by

$$\begin{aligned} \alpha_m(\zeta) &= \cos\big((m-1)\pi \sin(\zeta)\big) \\ \beta_m(\zeta) &= \sin\big((m-1)\pi \sin(\zeta)\big). \end{aligned} \tag{7}$$

The channel phase-offset is modeled by the rotation matrix

$$\boldsymbol{\Phi}(\phi) = \begin{bmatrix} \cos(\phi) & -\sin(\phi) \\ \sin(\phi) & \cos(\phi) \end{bmatrix} \in \mathbb{R}^{2\times 2}. \tag{8}$$

The transmit signal of the GNSS satellite consists of an in-phase and a quadrature transmit component

$$\boldsymbol{x}(t) = \begin{bmatrix} \sqrt{\rho C} x_I(t) & \sqrt{(1-\rho)C} x_Q(t) \end{bmatrix}^T \in \mathbb{R}^2, \tag{9}$$

where C is the carrier power in Watts and $0 \leq \rho \leq 1$ determines the power allocation between the in-phase and quadrature component. The interference signals $z_{I/Q}(t)$

$$\boldsymbol{z}(t) = \begin{bmatrix} z_I(t) & z_Q(t) \end{bmatrix}^T \in \mathbb{R}^2, \tag{10}$$

are approximated as independent, temporally white and wide-sense stationary Gaussian random processes with bandwidth B_J and flat power spectral density $\frac{N_J}{2}$ Watts per Hertz. Similar the sensor noise

$$\boldsymbol{\eta}(t) = \begin{bmatrix} \boldsymbol{\eta}_I^T(t) & \boldsymbol{\eta}_Q^T(t) \end{bmatrix}^T \in \mathbb{R}^{2M} \tag{11}$$

consists of $2M$ independent and wide-sense stationary Gaussian random processes

$$\boldsymbol{\eta}_{I/Q}(t) = \begin{bmatrix}\eta_{I/Q,1}(t) & \eta_{I/Q,2}(t) & \dots & \eta_{I/Q,M}(t)\end{bmatrix}^T \quad (12)$$

with flat power spectral density $\frac{N_0}{2}$ Watts per Hertz.

B. Sampling Process

Band-limiting the $2M$ analog receive signals $\boldsymbol{y}(t)$ by ideal low-pass filters with one-sided bandwidth B and sampling at a rate of $f_s = \frac{1}{T_s}$ with $f_s \geq 2B$, results in a digital receive signal of the form

$$\begin{aligned}\boldsymbol{y} &= (\boldsymbol{A}(\zeta_S) \otimes \mathbf{1}_N)\boldsymbol{x}(\tau_S) + \gamma_P(\boldsymbol{A}(\zeta_P)\boldsymbol{\Phi}(\phi_P) \otimes \mathbf{1}_N)\boldsymbol{x}(\tau_P) + \\ &\quad + (\boldsymbol{A}(\zeta_J) \otimes \mathbf{1}_N)\boldsymbol{z} + \boldsymbol{\eta} \\ &= \boldsymbol{s}(\boldsymbol{\theta}) + \boldsymbol{w}, \end{aligned} \quad (13)$$

where we summarize the channel parameters in the vector

$$\boldsymbol{\theta} = \begin{bmatrix}\zeta_S & \tau_S & \zeta_P & \phi_P & \tau_P & \zeta_J\end{bmatrix}^T \in \mathbb{R}^6 \quad (14)$$

and for notational convenience use

$$\begin{aligned}\boldsymbol{s}(\boldsymbol{\theta}) &= (\boldsymbol{A}(\zeta_S) \otimes \mathbf{1}_N)\boldsymbol{x}(\tau_S) + \gamma_P(\boldsymbol{A}(\zeta_P)\boldsymbol{\Phi}(\phi_P) \otimes \mathbf{1}_N)\boldsymbol{x}(\tau_P) \\ \boldsymbol{w} &= (\boldsymbol{A}(\zeta_J) \otimes \mathbf{1}_N)\boldsymbol{z} + \boldsymbol{\eta}. \end{aligned} \quad (15)$$

The entries of the signal vectors are given by

$$\begin{aligned}\boldsymbol{x}(\tau) &= \begin{bmatrix}\boldsymbol{x}_I^T(\tau) & \boldsymbol{x}_Q^T(\tau)\end{bmatrix}^T \\ \boldsymbol{z} &= \begin{bmatrix}\boldsymbol{z}_I^T & \boldsymbol{z}_Q^T\end{bmatrix}^T \\ \boldsymbol{\eta} &= \begin{bmatrix}\boldsymbol{\eta}_I^T & \boldsymbol{\eta}_Q^T\end{bmatrix}^T \\ \boldsymbol{\eta}_{I/Q} &= \begin{bmatrix}\boldsymbol{\eta}_{I/Q,1}^T & \boldsymbol{\eta}_{I/Q,2}^T & \dots & \boldsymbol{\eta}_{I/Q,M}^T\end{bmatrix}^T, \end{aligned} \quad (16)$$

with

$$\begin{aligned}\boldsymbol{x}_I(\tau) &= \begin{bmatrix}x_I(-\tau) & \dots & x_I((N-1)T_s - \tau)\end{bmatrix}^T \\ \boldsymbol{x}_Q(\tau) &= \begin{bmatrix}x_Q(-\tau) & \dots & x_Q((N-1)T_s - \tau)\end{bmatrix}^T \\ \boldsymbol{z}_{I/Q}(\tau) &= \begin{bmatrix}z_{I/Q}(0) & \dots & z_{I/Q}((N-1)T_s)\end{bmatrix}^T \\ \boldsymbol{\eta}_{I/Q}(\tau) &= \begin{bmatrix}\eta_{I/Q}(0) & \dots & \eta_{I/Q}((N-1)T_s)\end{bmatrix}^T. \end{aligned} \quad (17)$$

The covariance matrix of the random interference is

$$\begin{aligned}\boldsymbol{R}_z(\zeta_J) &= (\boldsymbol{A}(\zeta_J) \otimes \mathbf{1}_N)\,\mathrm{E}\left[\boldsymbol{z}\boldsymbol{z}^T\right](\boldsymbol{A}(\zeta_J) \otimes \mathbf{1}_N)^T \\ &= (\boldsymbol{A}(\zeta_J) \otimes \mathbf{1}_N)(\mathbf{1}_2 \otimes \boldsymbol{T}_z)(\boldsymbol{A}(\zeta_J) \otimes \mathbf{1}_N)^T \\ &= \boldsymbol{A}(\zeta_J)\boldsymbol{A}^T(\zeta_J) \otimes \boldsymbol{T}_z, \end{aligned} \quad (18)$$

while for the sensor noise

$$\begin{aligned}\boldsymbol{R}_\eta &= \mathrm{E}\left[\boldsymbol{\eta}\boldsymbol{\eta}^T\right] \\ &= \mathbf{1}_{2M} \otimes \boldsymbol{T}_\eta. \end{aligned} \quad (19)$$

The entries of the temporal covariance matrices $\boldsymbol{T}_z$ and $\boldsymbol{T}_\eta$ depend on the signal bandwidth and the sampling rate

$$\begin{aligned}[\boldsymbol{T}_z]_{ij} &= B_z N_J \,\mathrm{sinc}\left(2B_z T_s|i-j|\right) \\ [\boldsymbol{T}_\eta]_{ij} &= BN_0 \,\mathrm{sinc}\left(2BT_s|i-j|\right). \end{aligned} \quad (20)$$

where $B_z = \min(B_J, B)$. With the assumption that the interference $\boldsymbol{z}$ and the sensor noise $\boldsymbol{\eta}$ are independent, the overall covariance of the receive signal (13) is given by

$$\begin{aligned}\boldsymbol{R}(\boldsymbol{\theta}) &= \mathrm{E}\left[\boldsymbol{w}\boldsymbol{w}^T\right] \\ &= \boldsymbol{R}_z(\zeta_J) + \boldsymbol{R}_\eta \\ &= \boldsymbol{A}(\zeta_J)\boldsymbol{A}^T(\zeta_J) \otimes \boldsymbol{T}_z + \mathbf{1}_{2M} \otimes \boldsymbol{T}_\eta. \end{aligned} \quad (21)$$

C. Amplitude Quantization

In the following we assume, that the ADC for each of the M output channels is a symmetric hard-limiter, such that the final digital receive data $\boldsymbol{r} \in \{-1, 1\}^{2MN}$ is

$$\boldsymbol{r} = \mathrm{sign}\left(\boldsymbol{y}\right), \quad (22)$$

where the element-wise signum-function is defined

$$[\mathrm{sign}(\boldsymbol{y})]_i = \begin{cases}+1 & \text{if } \boldsymbol{y}_i \geq 0 \\ -1 & \text{if } \boldsymbol{y}_i < 0. \end{cases} \quad (23)$$

III. Performance Measure

In order to discuss the performance of the receiver in a compact analytical way, it is assumed that the maximum-likelihood estimator (MLE)

$$\hat{\boldsymbol{\theta}}(\boldsymbol{r}) = \arg\max_{\boldsymbol{\theta}} \ln p(\boldsymbol{r}; \boldsymbol{\theta}) \quad (24)$$

is used for estimation of the channel parameters $\boldsymbol{\theta}$. As the MLE is asymptotically unbiased and efficient, the mean square error matrix

$$\boldsymbol{R}_{\mathrm{MSE}}(\boldsymbol{\theta}) = \mathrm{E}\left[\left(\hat{\boldsymbol{\theta}}(\boldsymbol{r}) - \boldsymbol{\theta}\right)\left(\hat{\boldsymbol{\theta}}(\boldsymbol{r}) - \boldsymbol{\theta}\right)^T\right], \quad (25)$$

for sufficiently many samples N can be characterized through the inverse of the Fisher information matrix (FIM)

$$\boldsymbol{R}_{\mathrm{MSE}}(\boldsymbol{\theta}) = \boldsymbol{F}^{-1}(\boldsymbol{\theta}), \quad (26)$$

also known as the Cramér-Rao lower bound (CRLB). The FIM is defined by

$$\boldsymbol{F}(\boldsymbol{\theta}) = \int_{\mathcal{R}} p(\boldsymbol{r}; \boldsymbol{\theta}) \left(\frac{\partial \ln p(\boldsymbol{r}; \boldsymbol{\theta})}{\partial \boldsymbol{\theta}}\right)^2 \mathrm{d}\boldsymbol{r}, \quad (27)$$

where $\mathcal{R}$ is the support of the binary receive vector $\boldsymbol{r}$.

A. Pessimistic Performance Characterization

As the analytic description of $\boldsymbol{F}(\boldsymbol{\theta})$ is difficult for signal models with noise correlation, in the following an approximation $\tilde{\boldsymbol{F}}(\boldsymbol{\theta})$ of the FIM is used which exhibits the property

$$\boldsymbol{F}(\boldsymbol{\theta}) \succeq \tilde{\boldsymbol{F}}(\boldsymbol{\theta}), \quad (28)$$

and therefore assures that $\tilde{\boldsymbol{F}}(\boldsymbol{\theta})$ yields a pessimistic performance characterization. With the parametric moments

$$\begin{aligned}\boldsymbol{\mu}(\boldsymbol{\theta}) &= \int_{\mathcal{R}} \boldsymbol{r} p(\boldsymbol{r}; \boldsymbol{\theta}) \mathrm{d}\boldsymbol{r} \\ \boldsymbol{C}(\boldsymbol{\theta}) &= \int_{\mathcal{R}} \left(\boldsymbol{r} - \boldsymbol{\mu}(\boldsymbol{\theta})\right)\left(\boldsymbol{r} - \boldsymbol{\mu}(\boldsymbol{\theta})\right)^T p(\boldsymbol{r}; \boldsymbol{\theta}) \mathrm{d}\boldsymbol{r}, \end{aligned} \quad (29)$$

a pessimistic form of the FIM is given by [15]

$$\tilde{\boldsymbol{F}}(\boldsymbol{\theta}) = \left(\frac{\partial \boldsymbol{\mu}(\boldsymbol{\theta})}{\partial \boldsymbol{\theta}}\right)^T \boldsymbol{C}^{-1}(\boldsymbol{\theta}) \left(\frac{\partial \boldsymbol{\mu}(\boldsymbol{\theta})}{\partial \boldsymbol{\theta}}\right). \tag{30}$$

The first moment can be calculated element-wise by

$$[\boldsymbol{\mu}(\boldsymbol{\theta})]_i = \operatorname{erf}\left(\frac{[\boldsymbol{s}(\boldsymbol{\theta})]_i}{\sqrt{2[\boldsymbol{R}(\boldsymbol{\theta})]_{ii}}}\right), \tag{31}$$

where $\operatorname{erf}(z)$ is the error-function. Further, the diagonal of the second moment is found by calculating

$$[\boldsymbol{C}(\boldsymbol{\theta})]_{ii} = 1 - [\boldsymbol{\mu}(\boldsymbol{\theta})]_i^2, \tag{32}$$

while the off-diagonal entries are given by

$$[\boldsymbol{C}(\boldsymbol{\theta})]_{ij} = 4\Phi_{ij}(\boldsymbol{\theta}) - \big(1 - [\boldsymbol{\mu}(\boldsymbol{\theta})]_i\big)\big(1 - [\boldsymbol{\mu}(\boldsymbol{\theta})]_j\big), \tag{33}$$

where $\Phi_{ij}(\boldsymbol{\theta})$ is the cumulative density function (CDF) for the bivariate Gaussian distribution

$$p(\zeta_i, \zeta_j) = \mathcal{N}\left(\begin{bmatrix}0\\0\end{bmatrix}, \begin{bmatrix}[\boldsymbol{R}(\boldsymbol{\theta})]_{ii} & [\boldsymbol{R}(\boldsymbol{\theta})]_{ij}\\ [\boldsymbol{R}(\boldsymbol{\theta})]_{ji} & [\boldsymbol{R}(\boldsymbol{\theta})]_{jj}\end{bmatrix}\right) \tag{34}$$

with upper integration boarder $\begin{bmatrix}-[\boldsymbol{s}(\boldsymbol{\theta})]_i & -[\boldsymbol{s}(\boldsymbol{\theta})]_j\end{bmatrix}^T$. The derivative of the first moment is found element-wise by

$$\left[\frac{\partial \boldsymbol{\mu}(\boldsymbol{\theta})}{\partial \boldsymbol{\theta}}\right]_i = \sqrt{\frac{2}{\pi}} \frac{\mathrm{e}^{-\frac{[\boldsymbol{s}(\boldsymbol{\theta})]_i^2}{2[\boldsymbol{R}(\boldsymbol{\theta})]_{ii}}}}{\sqrt{[\boldsymbol{R}(\boldsymbol{\theta})]_{ii}}} \left(\frac{\partial [\boldsymbol{s}(\boldsymbol{\theta})]_i}{\partial \boldsymbol{\theta}} - \right. \\ \left. - \frac{[\boldsymbol{s}(\boldsymbol{\theta})]_i}{2[\boldsymbol{R}(\boldsymbol{\theta})]_{ii}} \frac{\partial [\boldsymbol{R}(\boldsymbol{\theta})]_{ii}}{\partial \boldsymbol{\theta}}\right), \tag{35}$$

with the derivatives

$$\frac{\partial [\boldsymbol{s}(\boldsymbol{\theta})]_i}{\partial \boldsymbol{\theta}} = \Big[\frac{\partial [\boldsymbol{s}(\boldsymbol{\theta})]_i}{\partial \zeta_S} \quad \frac{\partial [\boldsymbol{s}(\boldsymbol{\theta})]_i}{\partial \tau_S} \quad \frac{\partial [\boldsymbol{s}(\boldsymbol{\theta})]_i}{\partial \zeta_P} \\ \frac{\partial [\boldsymbol{s}(\boldsymbol{\theta})]_i}{\partial \phi_P} \quad \frac{\partial [\boldsymbol{s}(\boldsymbol{\theta})]_i}{\partial \tau_P} \quad \frac{\partial [\boldsymbol{s}(\boldsymbol{\theta})]_i}{\partial \zeta_J}\Big]$$

$$\begin{aligned}
\frac{\partial \boldsymbol{s}(\boldsymbol{\theta})}{\partial \zeta_S} &= \Big(\frac{\partial \boldsymbol{A}(\zeta_S)}{\partial \zeta_S} \otimes \mathbf{1}_N\Big)\boldsymbol{x}(\tau_S)\\
\frac{\partial \boldsymbol{s}(\boldsymbol{\theta})}{\partial \tau_S} &= \big(\boldsymbol{A}(\zeta_S) \otimes \mathbf{1}_N\big)\frac{\partial \boldsymbol{x}(\tau_S)}{\partial \tau_S}\\
\frac{\partial \boldsymbol{s}(\boldsymbol{\theta})}{\partial \zeta_P} &= \gamma_P\Big(\frac{\partial \boldsymbol{A}(\zeta_P)}{\partial \zeta_P}\boldsymbol{\Phi}(\phi_P) \otimes \mathbf{1}_N\Big)\boldsymbol{x}(\tau_P)\\
\frac{\partial \boldsymbol{s}(\boldsymbol{\theta})}{\partial \phi_P} &= \gamma_P\Big(\boldsymbol{A}(\zeta_P)\frac{\partial \boldsymbol{\Phi}(\phi_P)}{\partial \phi_P} \otimes \mathbf{1}_N\Big)\boldsymbol{x}(\tau_P)\\
\frac{\partial \boldsymbol{s}(\boldsymbol{\theta})}{\partial \tau_P} &= \gamma_P\big(\boldsymbol{A}(\zeta_P)\boldsymbol{\Phi}(\phi_P) \otimes \mathbf{1}_N\big)\frac{\partial \boldsymbol{x}(\tau_P)}{\partial \tau_P}\\
\frac{\partial \boldsymbol{s}(\boldsymbol{\theta})}{\partial \zeta_J} &= \mathbf{0}\\
\frac{\partial \boldsymbol{\Phi}(\phi)}{\partial \phi} &= \begin{bmatrix}-\sin(\phi) & \cos(\phi)\\ -\cos(\phi) & -\sin(\phi)\end{bmatrix}\\
\frac{\partial [\boldsymbol{R}(\boldsymbol{\theta})]_{ii}}{\partial \boldsymbol{\theta}} &= \begin{bmatrix}0 & 0 & 0 & 0 & 0 & \frac{\partial [\boldsymbol{R}_z(\zeta_J)]_{ii}}{\partial \zeta_J}\end{bmatrix}.
\end{aligned} \tag{36}$$

The derivatives of the transmit signal associated with the time-delay are found by

$$\begin{aligned}
\frac{\partial \boldsymbol{x}(\tau)}{\partial \tau} &= \begin{bmatrix}\frac{\partial \boldsymbol{x}_I^T(\tau)}{\partial \tau} & \frac{\partial \boldsymbol{x}_Q^T(\tau)}{\partial \tau}\end{bmatrix}^T\\
\frac{\partial [\boldsymbol{x}_{I/Q}(\tau)]_i}{\partial \tau} &= -\frac{\mathrm{d}x_{I/Q}(t)}{\mathrm{d}t}\Big|_{t=(i-1)T_s-\tau}.
\end{aligned} \tag{37}$$

Note, that the entries of the exact FIM for an ideal receiver which has access to the data $\boldsymbol{y}$ with infinite resolution is [14]

$$[\boldsymbol{F}_\infty(\boldsymbol{\theta})]_{ij} = \left(\frac{\partial \boldsymbol{s}(\boldsymbol{\theta})}{\partial [\boldsymbol{\theta}]_i}\right)^T \boldsymbol{R}^{-1}(\boldsymbol{\theta}) \left(\frac{\partial \boldsymbol{s}(\boldsymbol{\theta})}{\partial [\boldsymbol{\theta}]_j}\right) \\ + \frac{1}{2}\operatorname{tr}\left(\boldsymbol{R}^{-1}(\boldsymbol{\theta})\frac{\partial \boldsymbol{R}(\boldsymbol{\theta})}{\partial [\boldsymbol{\theta}]_i}\boldsymbol{R}^{-1}(\boldsymbol{\theta})\frac{\partial \boldsymbol{R}(\boldsymbol{\theta})}{\partial [\boldsymbol{\theta}]_j}\right). \tag{38}$$

IV. Reference System and Relative Performance

In order to analyze the potential of 1-bit GNSS receivers with multiple antennas and high sampling rates, we will compare the achievable ranging accuracy of different receive setups to an ideal reference system with infinite ADC resolution.

A. Ideal Reference System

In all scenarios the transmitter is a satellite of the American GPS system sending C/A - L1 signals [16] with a symbol duration of $T_c = \frac{1}{f_c}$ at a carrier frequency of 1575.42 MHz. The reference frequency of the system is $f_c = 1.023$MHz. The transmit signal is limited to a one-sided bandwidth of $B_t = 11.253$ MHz (main-lobe and 5 side-lobes) at the satellite and a I/Q power allocation of $\rho = 1$ is assumed. For the reference receive system with infinite ADC resolution, we assume $M = 2$ antennas and a receive strength of $C/N_0 = 45.0$ dB at each sensor. After demodulation to baseband, the ideal reference receiver band-limits the receive signal of each antenna to a one-sided bandwidth of $B_r = 1.023$ MHz (main lobe) by using an ideal low-pass filter and samples at a rate of $f_s = 2.046$ MHz with infinite ADC resolution for a duration of $T_o = 1$ ms.

B. Relative Performance

In the following the focus will lie on the accuracy of the pseudo-range measurement $\hat{\tau}_S$ for a single satellite which is given by

$$\operatorname{MSE}(\hat{\tau}_S) = \big[\boldsymbol{F}^{-1}(\boldsymbol{\theta})\big]_{22} \tag{39}$$

and is directly related to the accuracy of the final positioning solution of the GNSS system, which is calculated from the pseudo-range measurements of all in-view satellites. In order to compare different receive systems with infinite ADC resolution to the reference system, we introduce the relative performance measure

$$\chi_\infty = 10\log\left(\frac{\big[\boldsymbol{F}_\infty^{-1}(\boldsymbol{\theta})\big]_{22}}{\big[\boldsymbol{F}_{\text{REF}}^{-1}(\boldsymbol{\theta})\big]_{22}}\right), \tag{40}$$

while for a comparison of a receive system with 1-bit ADC to the reference system the relative performance measure

$$\chi_{\text{1-bit}} = 10\log\left(\frac{\left[\tilde{\boldsymbol{F}}^{-1}(\boldsymbol{\theta})\right]_{22}}{\left[\boldsymbol{F}_{\text{REF}}^{-1}(\boldsymbol{\theta})\right]_{22}}\right), \tag{41}$$

is used. These relative performance measures allow to characterize the gain or loss as equivalent SNR. For example, a system which exhibits $\chi = 3.0$ dB attains the same performance as the reference system with the satellite using the double amount of transmit power. Note that in such case the root mean square error (RMSE) of the positioning solution is diminished accordingly by a factor of $\frac{1}{\sqrt{2}}$.

V. GNSS Performance Analysis

For the analysis we consider three different scenarios:

A. Line-of-Sight Scenario

The first scenario assumes a simple line-of-sight receive situation without multi-path and interference (see Fig. 2). In

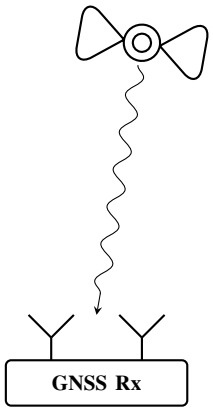

Fig. 2. Line-of-sight GNSS receive setup

this case, the receive signal model (13) simplifies to

$$\begin{aligned}\boldsymbol{y} &= (\boldsymbol{A}(\zeta_S) \otimes \mathbf{1}_N)\boldsymbol{x}(\tau_S) + \boldsymbol{\eta} \\ &= \boldsymbol{s}(\boldsymbol{\theta}) + \boldsymbol{\eta},\end{aligned} \tag{42}$$

where the channel parameters are

$$\boldsymbol{\theta} = \begin{bmatrix}\zeta_S & \tau_S\end{bmatrix}^T. \tag{43}$$

The angle of the direct path is $\zeta_S = 0$. In order to visualize the performance in correspondence with the number of receive antennas M, Fig. 3 visualizes χ_∞, where a system with M antennas working at $B_r = 1.023$ MHz and sampling rate $f_s = 2B_r$ is compared to the reference system with $M = 2$. It can be observed that doubling the number of receive antennas results in a gain of $\chi = 3.0$ dB. This is also true for systems with 1-bit ADC, which show a performance $\chi_{\text{1-bit}}$ that lies in general -2.0 dB below the performance of receivers with ideal ADC. The result indicates that using a 1-bit GNSS receiver with $M = 3$ antennas allows to approximately attain the same performance than with the ideal reference system with $M = 2$

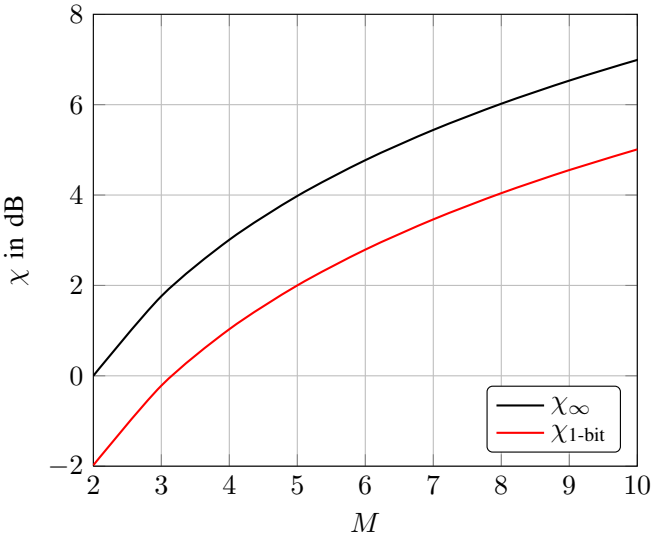

Fig. 3. Performance vs. number of antennas M

antennas. In contrast Fig. 4 shows the scaling behavior of the estimation performance as a function of the receive bandwidth κ. Therefore, under the relative performance measure χ_∞ an

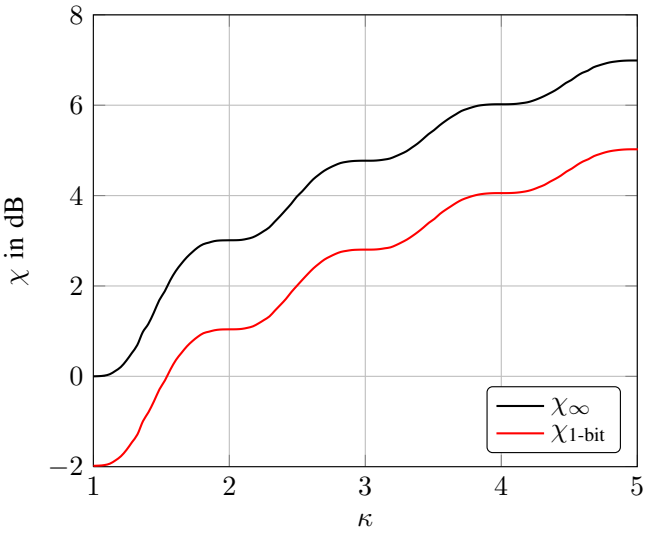

Fig. 4. Performance vs. receive bandwidth B_s

ideal receive system with infinite ADC resolution, $M = 2$ antennas, receive bandwidth $B_r = \kappa \cdot 1.023$ MHz, $\kappa \geq 1$ and sampling rate $f_s = 2B_r$ is compared to the reference system operating at $\kappa = 1$. In parallel the figure of merit $\chi_{\text{1-bit}}$ is depicted to show the relative performance of a system with 1-bit ADC. Interestingly, it is observed that the receive bandwidth is a crucial design criterion for high-performance GNSS systems as it allows to increase the performance of the positioning solution significantly. This is due to the fact that for the Fisher information of the time-delay parameter τ_S the SNR exhibits a quadratic weight with respect to the frequency. As the spectral power density of the satellite signal,

and consequently the SNR decays quadratic with frequency, a linear growth of the accuracy, similar to the case with M antennas, is observed. The 1-bit GNSS receive systems benefit from the same effect while their performance $\chi_{\text{1-bit}}$ in this scenario lies constantly -2.0 dB below the performance of the receivers with ideal ADC. Consequently, with 1-bit ADC sampling at a temporal rate of approximately $\kappa = 1.5$ is sufficient to outperform the ideal reference system with $\kappa = 1.0$.

B. Multi-path Scenario

The following scenario assumes that the GNSS satellite is received through the line-of-sight path with an additional multi-path component (see Fig. 5). The receive signal model

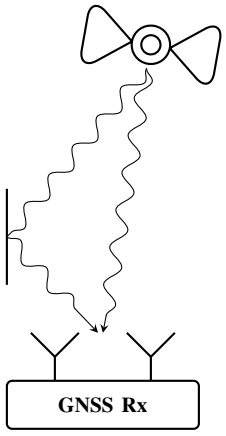

Fig. 5. GNSS receive setup with multi-path propagation

(13) therefore simplifies to

$$\begin{aligned}\boldsymbol{y} &= (\boldsymbol{A}(\zeta_S) \otimes \mathbf{1}_N)\boldsymbol{x}(\tau_S) + \gamma_P(\boldsymbol{A}(\zeta_P)\boldsymbol{\Phi}(\phi_P) \otimes \mathbf{1}_N)\boldsymbol{x}(\tau_P) + \boldsymbol{\eta} \\ &= \boldsymbol{s}(\boldsymbol{\theta}) + \boldsymbol{\eta} \end{aligned} \tag{44}$$

with the channel parameter vector

$$\boldsymbol{\theta} = \begin{bmatrix} \zeta_S & \tau_S & \zeta_P & \phi_P & \tau_P \end{bmatrix}. \tag{45}$$

The time-delays of the direct path and the multi-path component are chosen such that $\Delta\tau = \tau_P - \tau_S = 0.1T_c$ while the angles are $\zeta_S = 0$ and $\zeta_P = \frac{\pi}{16}$. The multi-path attenuation is set to $\gamma_P = 0.5$, i.e. -3.0 dB in comparison to the direct path, and the phase offset is $\phi_P = 0$. In order to investigate the GNSS performance scaling under multi-path propagation in correspondence with the number of antennas, Fig. 6 visualizes the relative performance χ_∞ with respect to an ideal receive system with infinite ADC resolution, $M = 2$ antennas, $B_r = 1.023$ MHz and sampling at a temporal rate $f_s = 2B_r$. It becomes clear that the positioning performance is increased substantially if a higher number of antennas M is used. In this specific GNSS scenario using $M = 6$ instead of $M = 2$ antennas with ideal ADC allows to attain the same performance as in a multi-path free scenario (MPF, dashed line). The 1-bit GNSS system with $M = 3$ antennas already outperforms the ideal reference system with $M = 2$

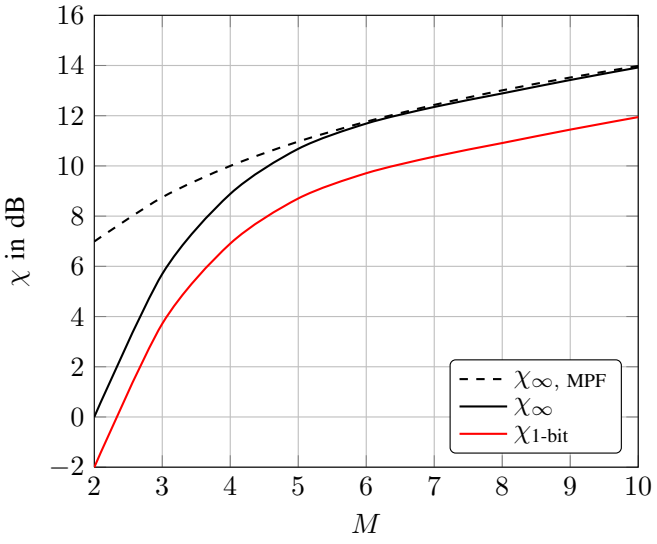

Fig. 6. Estimation performance versus number of antennas M

by $\chi_{\text{1-bit}} = 3.71$ dB under multi-path propagation. Fig. 7 shows a similar comparison where the performance scaling as a function of the receive bandwidth κ is visualized. With

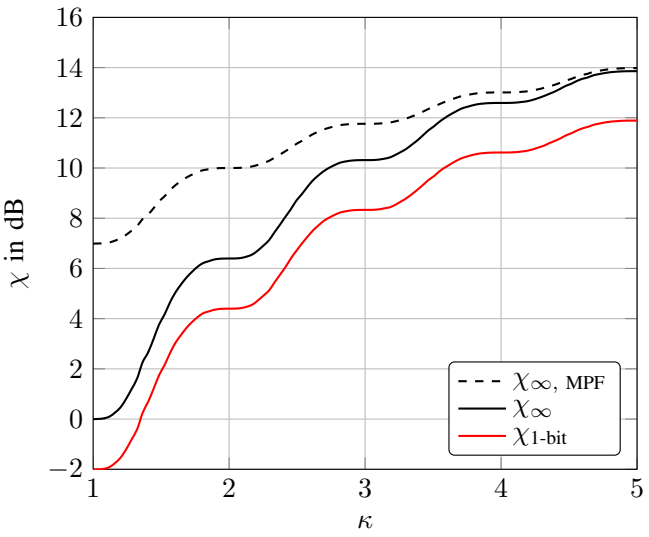

Fig. 7. Estimation performance versus receive bandwidth B_s

the performance measure χ_∞ an ideal receive system with infinite ADC resolution, $M = 2$ antennas, receive bandwidth $B_r = \kappa \cdot 1.023$ MHz, $\kappa \geq 1$ and sampling rate $f_s = 2B_r$ is compared to the reference system operating at $\kappa = 1$. It becomes obvious that also the receive bandwidth κ can be used to mitigate the effect of multi-path propagation. Increasing the receive bandwidth by factor $\kappa = 5$ with ideal ADC allows to attain the same performance as in a multi-path free scenario (MPF, dashed line). It is observed that in the considered case already with $\kappa = 1.35$ the 1-bit system outperforms the ideal reference receiver.

C. Broadband Interference Scenario

The third scenario assumes the reception of a single GNSS satellite through the line-of-sight path with additional broadband interference from a single signal source (see Fig. 8). The

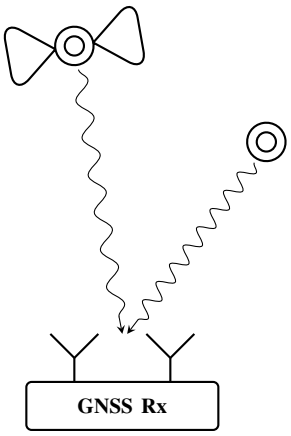

Fig. 8. GNSS receive setup with broadband interference

one-sided bandwidth of the interferer is assumed to be fixed to $B_J = 1.023$ MHz, while the power spectral density of the interference is $N_J = N_0$. In this situation the receive signal model (13) can be written

$$\begin{aligned} \boldsymbol{y} &= (\boldsymbol{A}(\zeta_S) \otimes \mathbf{1}_N)\boldsymbol{x}(\tau_S) + (\boldsymbol{A}(\zeta_J) \otimes \mathbf{1}_N)\boldsymbol{z} + \boldsymbol{\eta} \\ &= \boldsymbol{s}(\boldsymbol{\theta}) + \boldsymbol{\eta} \end{aligned} \tag{46}$$

with the channel parameters

$$\boldsymbol{\theta} = \begin{bmatrix} \zeta_S & \tau_S & \zeta_J \end{bmatrix}. \tag{47}$$

The angles are set to $\zeta_S = 0$ and $\zeta_J = \frac{\pi}{16}$. Also for this receive model we visualize the relative performance gain as function of the the number of antennas M. Fig. 9 shows χ_∞ for an ideal receive system with infinite ADC resolution, M antennas, $B_r = 1.023$ MHz and sampling rate $f_s = 2B_r$ in comparison to the reference system with $M = 2$. It can be observed that the number of receive antennas allows to fully mitigate the degradation due to interference for ideal receive systems if $M = 9$ or more antennas are used. Also in this scenario the 1-bit GNSS receiver with $M = 3$ antennas attains approximately the same performance as the ideal reference system with $M = 2$. Fig. 10 shows the performance scaling as a function of the receive bandwidth κ. χ_∞ is plotted for an ideal receive system with infinite ADC resolution, $M = 2$ antennas, receive bandwidth $B_r = \kappa \cdot 1.023$ MHz, $\kappa \geq 1$ and sampling rate $f_s = 2B_r$ in comparison to the ideal reference system operating at $\kappa = 1$. It is observed, that also in this scenario the receive bandwidth helps to mitigate the harmful effect of interference. At $\kappa = 5$ the performance gap between the ideal receive system with interference and the ideal receive system without active interferer (IF, dashed line) is less than 1 dB. Already at $\kappa = 1.35$ the 1-bit GNSS receive system outperforms the reference system with $\kappa = 1$.

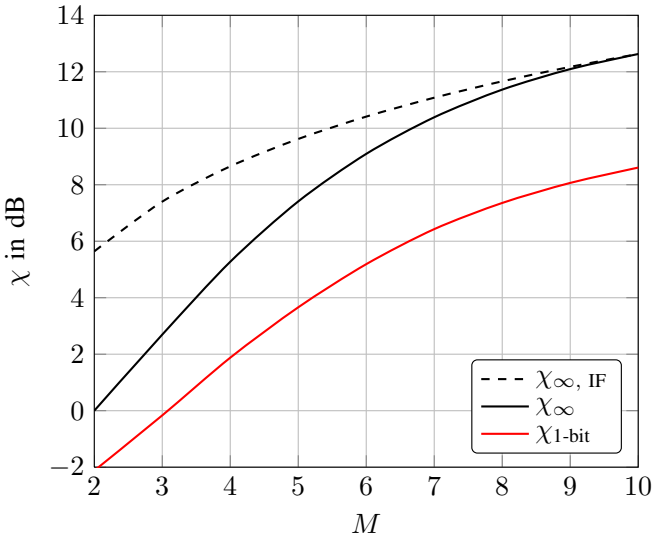

Fig. 9. Estimation performance versus number of antennas M

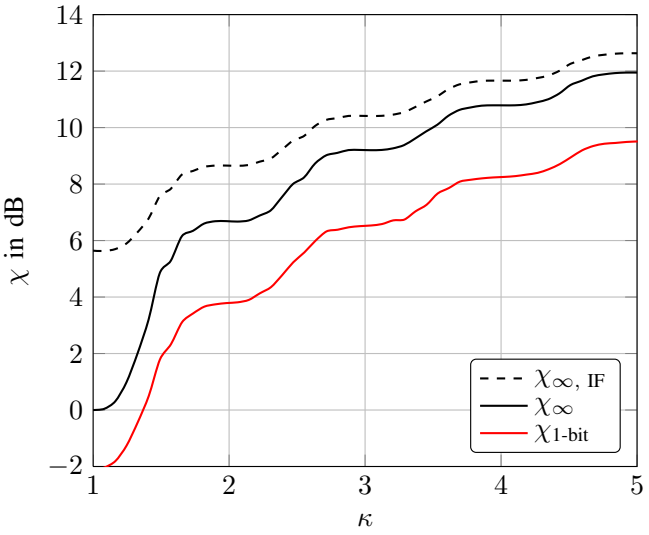

Fig. 10. Estimation performance versus receive bandwidth B_s

VI. Conclusion

We have carried out a far-reaching performance analysis of GNSS receive systems with ideal ADC and 1-bit ADC. The investigation of these two extreme cases under different numbers of receive antennas and bandwidths shows that these two design parameters are a key point for the development of robust high-performance GNSS receive systems. The resolution of the ADC plays only a secondary role. If a very simple symmetric 1-bit ADC is used, high receive bandwidth and multiple antennas can be realized in an energy and hardware-efficient way. The achievable performance gain clearly outweighs the loss that has to be taken into account due to the non-linearity of the ADC. Already increasing the number of antennas or the sampling rate by a factor of 1.5 allows to attain a positioning accuracy with 1-bit ADC

which is higher than with any other possible ADC resolution. Taking into account that for example a 2-bit ADC requires two comparators and an AGC for the low noise amplifier, shows that the energy and hardware budget of GNSS receive systems should not be invested into the resolution of the ADC but the number of receive sensors and the receive bandwidth, i.e. a fast temporal sampling rate. This will allow to build efficient and reliable high-performance receivers capable of coping with challenging GNSS receive situations like multi-path propagation and interference.

REFERENCES

[1] R. H. Walden, "Analog-to-digital converter survey and analysis," *IEEE J. Sel. Areas Commun.*, vol. 17, no. 4, pp.539–550, Apr. 1999.

[2] J. H. Van Vleck, D. Middleton, "The spectrum of clipped noise," *Proc. IEEE*, vol.54, no.1, pp. 2–19, Jan. 1966.

[3] R. Curry, "Estimation and Control with Quantized Measurements", *M.I.T Press*, 1970.

[4] T. M. Lok, V. K. W. Wei, "Channel Estimation with Quantized Observations", *IEEE International Symposium on Information Theory*, pp. 333, August 1998.

[5] M. T. Ivrlač, J. A. Nossek, "On Channel Estimation in Quantized MIMO Systems", *International ITG Workshop on Smart Antennas (WSA)*, 2007.

[6] A. Mezghani, F. Antreich, J.A. Nossek, "Multiple parameter estimation with quantized channel output", *International ITG Workshop on Smart Antennas (WSA)*, pp. 143 –150, 2010.

[7] T. Koch, A. Lapidoth, "Increased capacity per unit-cost by oversampling," *IEEE Conv. Electrical/Electronics Engineers Israel*, 2010, pp. 684–688.

[8] T. Koch and A. Lapidoth, At low SNR, asymmetric quantizers are better, *IEEE Trans. Inf. Theory*, vol. 59, no. 9, pp. 5421–5445, Sept. 2013.

[9] A. Mezghani, J.A. Nossek, "Capacity lower bound of MIMO channels with output quantization and correlated noise", IEEE International Symposium on Information Theory Proceedings (ISIT), 2012

[10] J. W. Betz , N. R. Shnidman "Receiver processing losses with bandlimiting and one-bit sampling", *Proceedings of the 20th International Technical Meeting of the Satellite Division of The Institute of Navigation (ION GNSS 2007)*, Texas, pp. 1244–1256, September 2007.

[11] J.T. Curran, D. Borio, G. Lachapelle, C.C. Murphy, "Reducing Front-End Bandwidth May Improve Digital GNSS Receiver Performance," *IEEE Trans. Signal Process.*, vol. 58, no. 4, pp.2399–2404, April 2010.

[12] M. Stein, F. Wendler, A. Mezghani, J. A. Nossek, "Quantization-loss reduction for signal parameter estimation," *Proc. IEEE Intern. Conf. Acoust., Speech and Signal Process.*, 2013, pp. 5800 – 5804.

[13] F. Wendler, M. Stein, A. Mezghani, J.A. Nossek, "Quantization-loss reduction for 1-bit BOC positioning", Proc. ION Intern. Technical Meeting (ITM), San Diego, January 2013

[14] S. M. Kay, "Fundamentals of Statistical Signal Processing: Estimation Theory," 1th ed. Upper Saddler River, NJ: Prentice Hall, 1993.

[15] M. Stein, A. Mezghani, J. A. Nossek, "A lower bound for the Fisher information measure," *IEEE Signal Process. Letters*, vol. 21, no. 7, pp. 796–799, July 2014.

[16] "NAVSTAR GPS Space Segment/Navigation User Interfaces," IS-GPS-200, Rev. D, ARINC Engineering Services, El Segundo, CA, 2004.